Supporting information

Unraveling the Interfacial Homogeneity and Bulk Crystallization for Efficient and Stable Perovskite Solar Cells via Ionic Liquids

Xiaowei Xu[a], Sibo Li[#b], Chengwei Shan[a], Xiaoyu Gu[a], Jie Zeng[c], Wenbo Peng[c], Tingting Dai[d], Xin Xu[a], Xianghui Zeng[e], Erjun Zhou[d], Chen Xie[e], Yong Zhang*[c,f], Longbin Qiu*[b], Baomin Xu*[c], Aung Ko Ko Kyaw*[a]

[a]Guangdong University Key Laboratory for Advanced Quantum Dot Displays and Lighting, and Department of Electronic & Electrical Engineering, Southern University of Science and Technology, Shenzhen 518055, PR China

[b]Shenzhen Key Laboratory of Intelligent Robotics and Flexible Manufacturing Systems, Department of Mechanical and Energy Engineering, SUSTech Energy Institute for Carbon Neutrality, Southern University of Science and Technology, Shenzhen 518055, China

[c]Department of Materials Science and Engineering, Southern University of Science and Technology, Shenzhen, Guangdong 518055, China.

[d]College of Biological, Chemical Sciences and Engineering, Jiaxing University, Jiaxing, Zhejiang 314001, China

[e]College of New Materials and New Energies, Shenzhen Technology University, Shenzhen 518118, China

[f]Sustainable Energy and Environment Thrust, Function Hub, The Hong Kong University of Science and Technology (Guangzhou), Nansha, Guangzhou, 511400 Guangdong, China

[#]These authors contributed equally

*Corresponding authors: Corresponding authors: Aung Ko Ko Kyaw, E-mail: aung@sustech.edu.cn; Longbin Qiu, E-mail: qiulb@sustech.edu.cn；Yong Zhang, E-mail: yongzhang@hkust-gz.edu.cn; Baomin Xu, E-mail: xubm@sustech.edu.cn

Table of contents

Experimental Section

Materials

All materials are commercially without purification unless specified. Formamidinium iodide (FAI) and nickel oxide (NiO_x) were purchased from Advanced Electron Technology CO., Ltd.. Methylammonium bromine (MABr) was purchased from Greatcell Solar Materials. Methylammonium chloride (MACl), cesium iodide (CsI) and 2-Thiopheneethylammonium chloride (TEACl) were bought from Xi'an e-Light New Material Co., Ltd.1,4-di(methylimidazolium)-butane dibromide and tetramethylguanidine tetrafluoroborate were purchased from Lanzhou Greenchem ILs. Co., Ltd. N, N-dimethylformamide (DMF), dimethylsulfoxide (DMSO) were bought from Alfa Aesar. Isopropanol (Ultradry 99.5%), methanol and ultradry ethanol were purchased from Sigma-Aldrich. Lead iodide (PbI_2) was purchased from Tokyo Chemical Industry (TCI). (4-(7H-dibenzo[c,g]carbazol-7-yl)butyl)phosphonic (4PADCB) were bought from Borun New Material. Lead bromide ($PbBr_2$), C60, and 2,9-dimethyl-4,7-diphenyl-1,10-phenanthroline (BCP) were purchased from Xi'an Polymer Light Technology Corp. Chlorobenzene (CB) and anhydrous ethanol were purchased from Aladdin. Silver grain was purchased from ZhongNuo Advanced Material (Beijing) Technology Co., Ltd. Poly(methyl methacrylate) (PMMA, M_w=150000) was purchased form Energy Chemistry.

Preparation of the perovskite precursor

226.7 mg FAI, 21.0 mg CsI, 7.8 mg MABr, 2.54 mg $PbBr_2$ and 661.3 mg PbI_2 and 12.0 mg MACl were dissolved in 1.0 mL mixed solvents (DMF: DMSO = 4:1, volume: volume). The perovskite precursor was stirred overnight at room temperature. To prepare the precursor solutions with $TMGBF_4$ (1,3, 5 mol% with respect to PbI_2), the additive was added to the DMF precursor solution.

Device fabrication

ITO/glass substrates (15 Ω sq^{-1} purchased from Advanced Electron Technology. CO., Ltd.) were sequentially ultrasonic cleaned in diluted detergent, deionized water (DI) water, isopropanol (IPA) and ethyl alcohol for 10 min sequentially and then dried in an oven. The pre-clean ITO glasses were treated with UV-Ozone for 25 min before depositing the hole transport layer. NiO_x dispersion (15 mg/mL in DI water) was sonicated for 6 min and then filtered with 0.22 μm polyether sulfone (PES) filter before usage. Afterwards, 40 μL of the dispersion was spin-coated on the ITO/glass substrate at a speed of 2000 rpm for 30 s, followed by an annealing at 200 °C for 25 min in air. After cooling, the substrates were transferred to a nitrogen-filled glove box. Then 4PADCB dissolved in anhydrous ethanol with a concentration of 0.5 mg/mL was spin-coated on NiO_x/ITO/glass at a speed of 3000 rpm for 30 s, followed by annealing at 120 °C for 12 min. After that, $Bu(MIm)_2Br_2$ (0.5 mg/mL dissolved in methanol) was dynamically spin-coated at a speed of 4000 rpm for 20 s, followed by annealing at 120 °C for 5 min. The perovskite precursor solution was filter by 0.22 μm PTFE filter and then spin-coated at a consecutive two-step process with 1000 rpm for 5 s followed by 4000 rpm for 25 s. During the second step, 200 μL of chlorobenzene was dropped on the substrate during the last 11 s of spin coating, and then annealed at 120 ℃ for 30 min. After cooling down, the substrate was treated with TEACl dissolved in a mixed solution (IPA: DMSO = 1000: 5. volume: volume, 0.8 mg/mL) at 4000 rpm for 30 s dynamically, followed by heat treatment at 120 ℃ for 5 min. Then the PMMA solution (0.5 mg/mL) was dynamically spin-coated on the films at 5000 rpm for 30 s. Finally, C60 (17 nm), BCP (7 nm) and Ag (80 nm) electrode was deposited by thermal evaporation with a mask area of 0.04 cm^2.

Device characterization

The *J-V* curves of the perovskite solar cells were measured with Keithley 2400 source meter under

1 sun (AM 1.5G spectrum) generated from a class solar simulator (Japan, SAN-EI, XES-40S1). The EQE spectrum was measured using a Solar Cell Spectral Response Measurement System QE-R3011 (Enlitech Co., Ltd.). The light intensity at each wavelength was calibrated using a standard single crystal Si photovoltaic cell. The stability of the unencapsulation device was tested under AM 1.5G illumination with light intensity of 100 mW/cm^2 in different condition. The dark current density was measured by the semiconductor parameter analyzer (Keithley 2400). The dynamic range measurements were performed under different intensities of monochromatic light using ThorLabs metallic coated neutral density filters. Capacitance-Voltage (CV) and Capacitance-frequence (C-f) measurements were performed with a frequency analyzer module-equipped potentiostat (PGSTAT302N, Autolab) in dark condition.

Sample characterization

The photoluminescence (PL) spectra and time-resolved (TRPL) were performed with a 532 nm laser driven by TektronixAGF1062A function generator integrated and a 350 MHz Tektronix MDO3034 oscilloscope. PL mapping was used in the Laser micro-confocal Raman spectrometer (LabRAM HR Evolution) with a 325 nm laser. The scanning electronic microscope (SEM) images were obtained from Apreo2 S Lovac field emission. The XPS and UPS spectra were recorded on ESCALab250Xi multifunction X-ray photoelectron spectrometer. The UV-vis absorption spectra were measured by Hitachi U-3010 spectrophotometer. Grazing incidence wide-angle X-ray scattering (GIWAXS) measurements were carried out with a Xenocs Xeuss 2.0 system with an Excillum etalJet-D2 X-ray source (70 kV, 2.857 mA, 1.341 Å) and a DECTRIS PILATUS3 R 1M area detector. The incidence angle is 0.2°. The ^{19}F and ^{1}H NMR measurements were performed on an AVANCE III 400M (Bruker). The surface and bottom roughness and potential were tested using a MultiMode 8-HR Atomic Force Microscope (AFM, Bruker) with a tapping amplitude modulation mode. Grazing incidence X-ray diffraction (GIXRD) patterns were acquired in air by using a Rigaku Smartlab with Cu Kα radiation (λ= 1.5405 Å). The femtosecond transient absorption measurements were performed on a Helios spectrometer (Ultrafast Systems) pumped by a Ti:sapphire regenerative amplifier (Legend Elite, Coherent) operating at 5 kHz with fundamental wavelength of 800 nm and pulse width of ~40 fs. The film samples were prepared on quartz and were selectively excited using 750 nm excitation at a fluence of 0.5 μJ cm^{-2} pulse, which corresponds to excitation densities on the order of ~10^{17} cm^{-3}.

The sample for the XPS tests were thinned down by GmbH, which was performed on ION TOF SIMS 5. Ar clusters (10 keV) were used in the sputtering. Bi^{3+} (30 keV) was used to probe the sample surface in the analysis phase.

Supplementary Note

1. Residual Stress Analysis

The film stress can be calculated according to the Bragg's Law and generalized Hooke's Law, the 2θ-$sin^2\Psi$ can be given by:[1]

$$\sigma = -\frac{E}{2(1+\upsilon)}\frac{\pi}{180}cot\theta_0\frac{\partial(2\theta)}{\partial sin^2\Psi} \quad (1)$$

where E and υ are Young's modulus (10 GPa) and Poisson's ratio of the perovskite film (0.3), respectively. θ_0 is the diffraction peak for strain-free perovskite crystal plane and θ is the diffraction peak for the measured perovskite films. ϕ is the angle of diffraction vector with respect to the sample normal direction.

2. Williamson-Hall Analysis

We calculated the variation of micro-strains according to the Williamson-Hall equation:[2]

$$\beta \times cos\theta = \frac{K\lambda}{D} + 4\varepsilon \times sin\theta \quad (2)$$

where D and ε represent the crystallite size and lattice distortion of perovskite films, respectively, β is the FWHM of diffraction peaks, θ is half of the scattering angle, *K* is the shape factor (0.9 for a cubic structure), λ is the wavelength of the incident X-rays (1.5406 Å)

3. Doping density (N_A) and space charge width (W)

The slopes of the *C-V* plots reflect the carrier concentration and the extrapolated intersection with the voltage axis yield the built-in voltage. The carrier concentration was calculated from the Mott-Schottky relation:[3]

$$N_A = \frac{-2}{q\varepsilon_r\varepsilon_0 A^2}\left(\frac{dV}{dC^{-2}}\right)^{-1} \quad (3)$$

where ε_r is the relative dielectric constant of perovskite (ε_r= 4/7), and the ε_0 is the dielectric constant of the vacuum, A is the device area. The space charge width (W) depends on the doping density and the built-in-voltage V_{bi} can be calculated by

$$W = \sqrt{\frac{2\varepsilon_r\varepsilon_0(V_{bi} - V)}{qN_A}} \quad (4)$$

where A is the active area, and V is the applied bias.

4. Light intensity-dependent V_{OC} analysis

$$V_{OC} = \frac{nk_BT}{q}\ln(I) + B \quad (5)$$

where k_B, *T, q, I, B* represent Boltzmann constant, thermodynamic temperature, the electron charge, light intensity and constant, respectively. The smaller n is theoretically, the indirect defect recombination at the interface (SRH recombination, Shockley-Read-Hall recombination) is smaller.

5. Admittance Spectroscopy analysis

The standard *C-V* and TAS measurements were performed by using was performed with a frequency analyser module-equipped potentiostat (PGSTAT302N, Autolab) in dark condition. For the standard *C-V* measurement, the DC bias was scanning from 0 V to 1.3 V for the perovskite solar cells. The Mott-Schottky curves were obtained by analysing the data in PIAOS software. For the TAS measurement, the DC bias was fixed at 0 V and the amplitude of the AC bias was 1.0 V. The scanning range of the AC frequency was 10 to 10^6 Hz.

The total trap density of states (tDOS) spectrum was calculated through the equation:[5, 6]

$$N_T(E_\omega) = -\frac{V_{bi}\omega dC}{W\ d\omega\ qk_BT}\ 1 \quad (6)$$

$$E_\omega = k_BTln\left(\frac{\beta T^2}{\omega}\right) \quad (7)$$

where q is the elementary charge, C is the capacitance, and ω is the applied angular frequency. V_{bi} and W are the built-in potential and the depletion width, respectively, which can be extracted from the Mott-Schottky analysis through the capacitance-voltage (*C*-*V*) measurement.

6. Activation energy (E_a) analysis

E_a values calculated by fitting the corresponding Arrhenius plots using the relation:

$$\omega_{peak} = \beta T^2 exp\left(-\frac{E_a}{k_B T}\right) \quad (8)$$

where β is a temperature-related parameter, T and k_B are the temperature and Boltzmann's constant, respectively. The characteristic transition frequency values (ω_{peak}) were obtained from the derivative of the capacitance-frequency spectra.

7. FF losses analysis

$$FF_{max} = \frac{v_{oc} - ln(v_{oc} + 0.72)}{v_{oc} + 1} \quad (9)$$

with $$v_{oc} = \frac{qV_{oc}}{nK_B T} \quad (10)$$

where K_B is Boltzmann's constant, T is Kelvin temperature and q is electron charge, n is ideality factor. The maximum FF is estimated without considering charge transport losses.

8. Calculation of quasi-Fermi level splitting (QFLS) based on the PL quantum yield (PLQY)

To investigate the non-radiative recombination perovskite film with and without $TMGBF_4$ treatment, we calculated the Quasi-Fermi level splitting (QFLS) values by using photoluminescence quantum yield (PLQY) measurements, which was conducted an FLS980 (Edinburgh Instruments Ltd.) by a 450.5 nm laser taken from the bottom ITO side inside an integrated sphere. According to the relation between QFLS and PLQY as the following equation:[7]

$$QFLS = QFLS_{rad} + k_B T \cdot ln(PLQY) = k_B T \cdot ln\left(PLQY \frac{J_G}{J_{0,rad}}\right) \quad (11)$$

where $QFLS_{rad}$ is the QFLS for the perovskite layer when only radiative recombination is present, k_B is the Boltzmann constant (1.38×10^{-23} J/K), and T is the temperature (300 K). J_G is the generation current density under illumination, in this case, approximated to the short-circuit current density J_{SC} of devices and $J_{0,rad}$ is the dark radiative recombination saturation current density.

According to the detailed balance theory, the $J_{0,rad}$ can be calculated by the following equations:

$$J_{0,rad} = q\int_0^\infty EQE_{PV}(E)\emptyset_{BB}(E)dE \tag{12}$$

$$\emptyset_{BB}(E) = \frac{2\pi E^2}{h^3c^2}\cdot\frac{1}{exp\left(\frac{E}{k_BT}\right)-1} \tag{13}$$

Where q is the elementary charge, EQE_{PV} is the photovoltaic external quantum efficiency, E is the photon energy, $\emptyset_{BB}$ is the black-body radiative spectrum, h is the Planck constant, and c is the light speed in a vacuum. $J_{0,rad}$ of perovskite filme without (Ref) and with (Target) is evaluated by EQE curves measured in **Figure S26**, which was calculated as 1.92×10^{-20} mA cm^{-2} for reference device and 1.63×10^{-20} mA cm^{-2} for target device, respectively. Subsequently, combined with the PLQY value, the corresponding QFLS of the samples with and without $TMGBF_4$ treatment are 1.209 and 1.204, respectively. Besides, the V_{OC} non-radiation recombination loss can be obtained by the following equation:

$$\Delta V_{OC}^{non-rad} = \frac{QFLS_{rad}-QFLS}{q} = -\frac{k_BTln(PLQY)}{q} \tag{14}$$

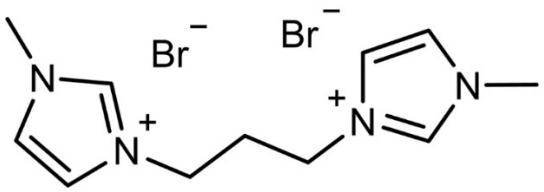

Figure S1. Chemical structure of 1,4-di(methylimidazolium)-butane dibromide ($Bu(MIm)_2Br_2$).

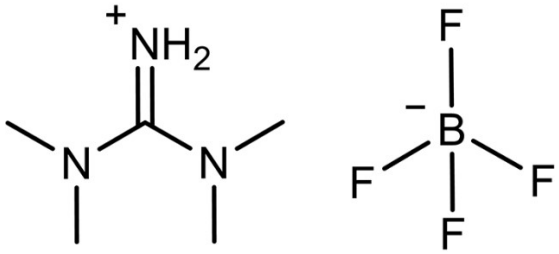

Figure S2. Chemical structure of tetramethylguanidine tetrafluoroborate ($TMGBF_4$).

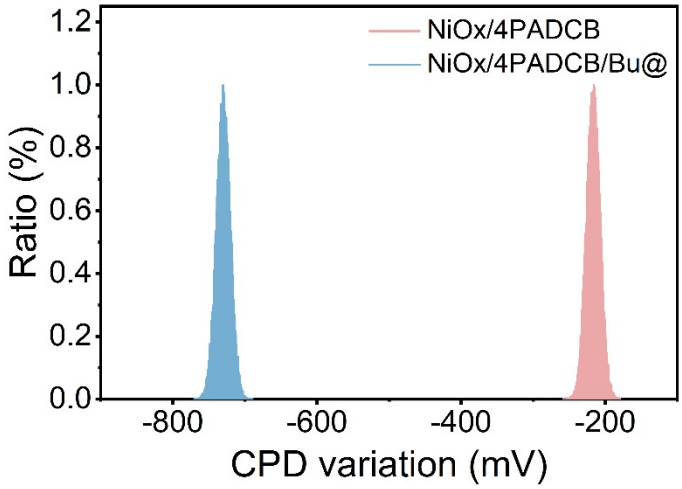

Figure S3. The statistical potential distributions of film surfaces.

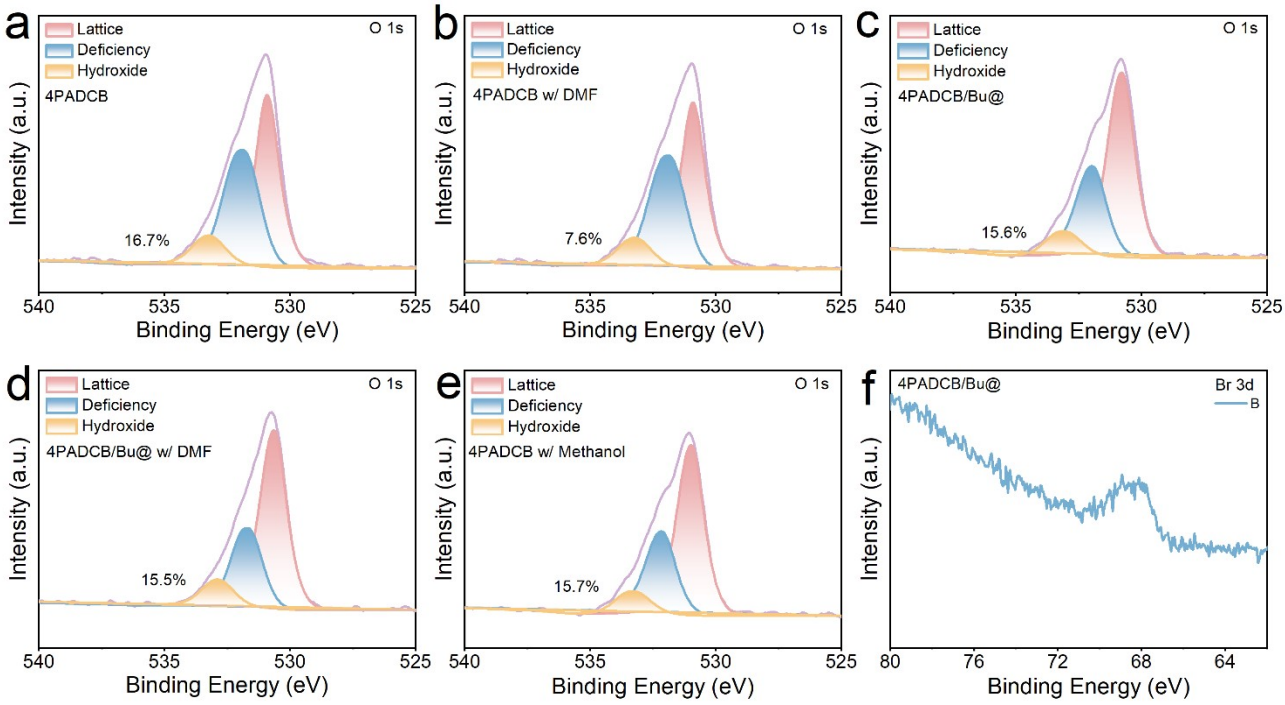

Figure S4. High-resolution XPS spectra of O 1s core levels of (a-d) ITO/4PADCB and ITO/4PADCB/Bu without and with DMF rise, respectively. (e) ITO/4PADCB with methanol rinse. (f) High-resolution XPS spectra of Br 3d.

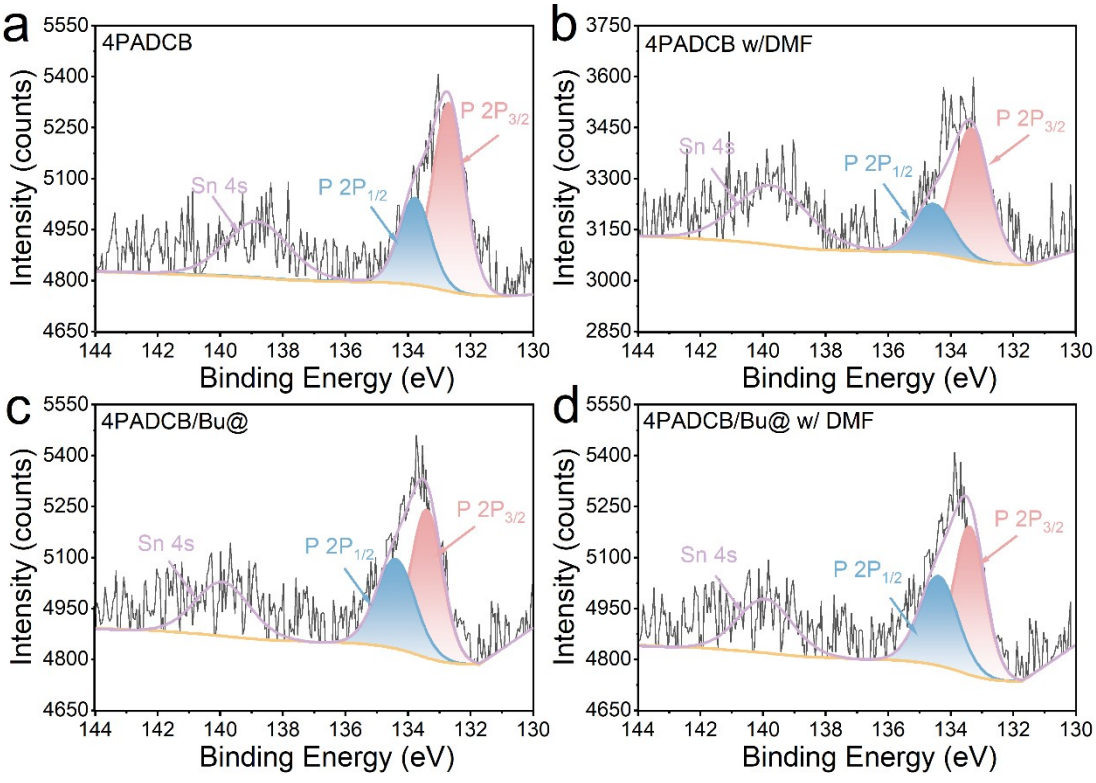

Figure S5. High-resolution XPS spectra of P 2p core levels of (a-b) ITO/4PADCB without and with

DMF rinse, respectively. (c-d) ITO/4PADCB/Bu without and with DMF rinse, respectively.

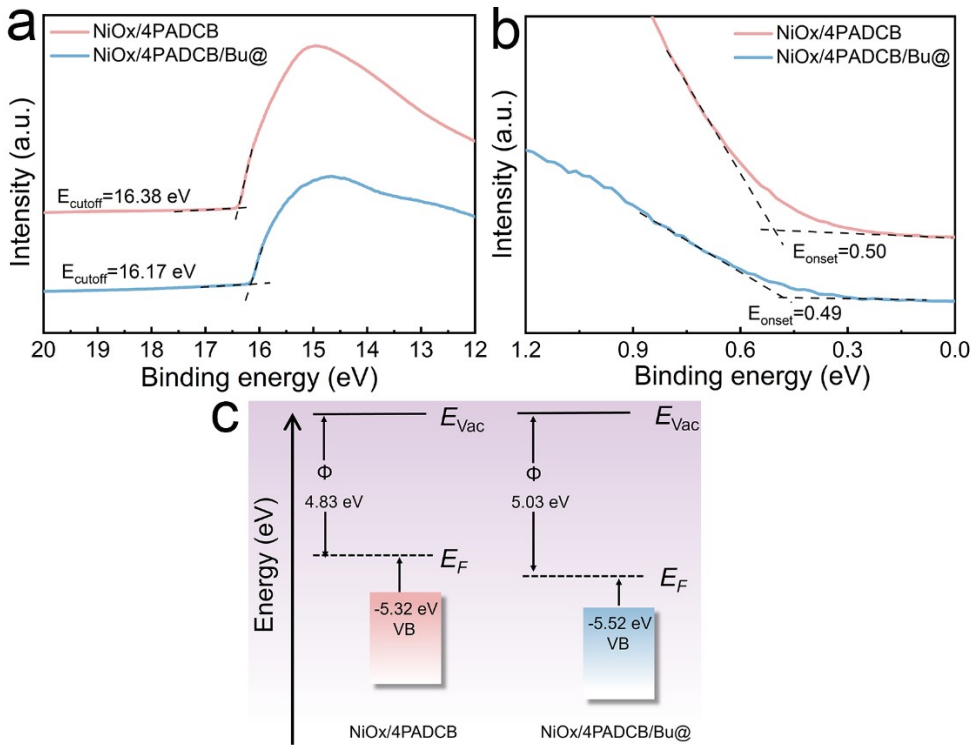

Figure S6. UPS spectra of (a) secondary electron cut-off and (b) valence bands for NiO_x/4PADCB and NiO_x/4PADCB/Bu@. (c) Schematic of adjustment of energy level alignment for for NiO_x/4PADCB and NiOx/4PADCB/Bu@, respectively.

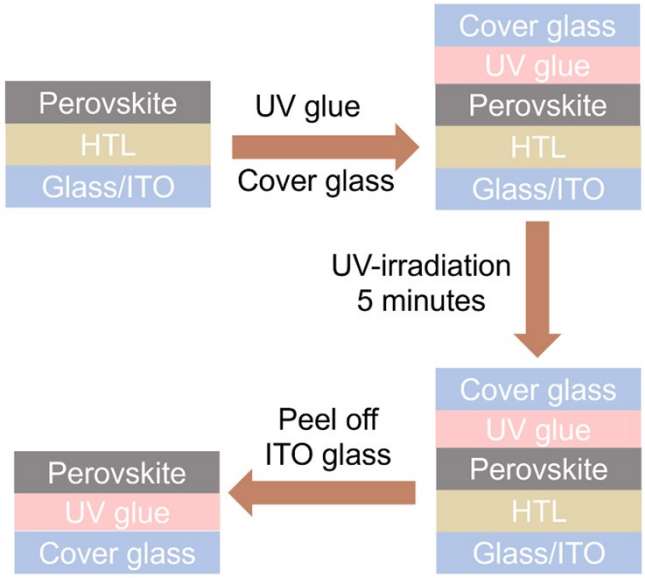

Figure S7. Schematic diagram of the bottom view for perovskite.

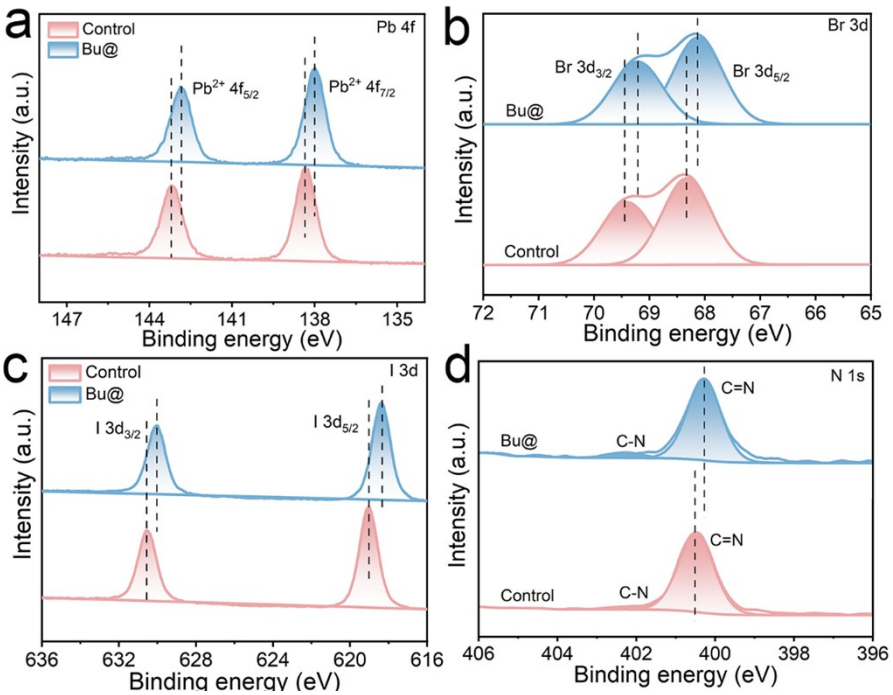

Figure S8. XPS spectra of (a) Pb 4f; (b) I 3d; (c) Br 3d and (d) N 1s of bottom-side of control and Bu@-treated perovskite films.

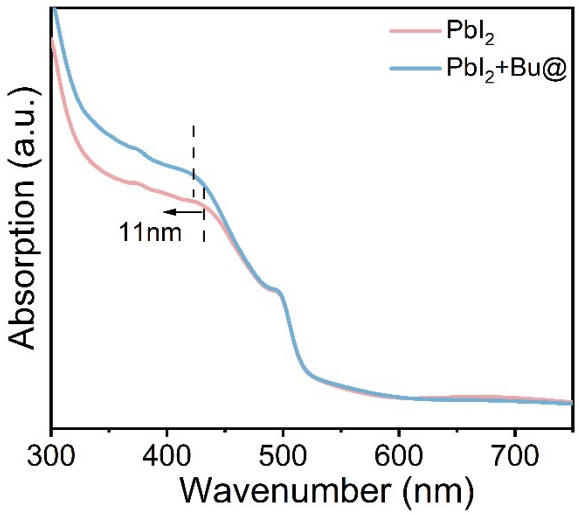

Figure S9. UV-vis absorption spectra of the neat PbI_2 film and PbI_2/Bu@ bilayer.

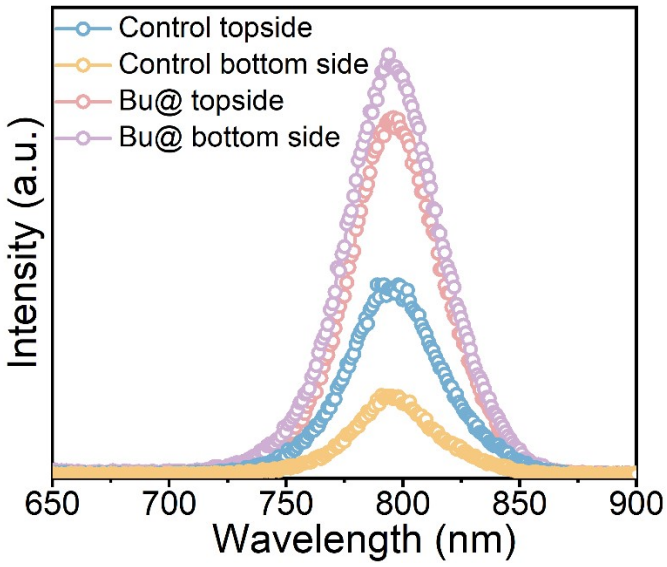

Figure S10. Steady-state PL spectra (excitation at 520 nm) of the control and Bu@-treated perovskite films excited from top and bottom sides.

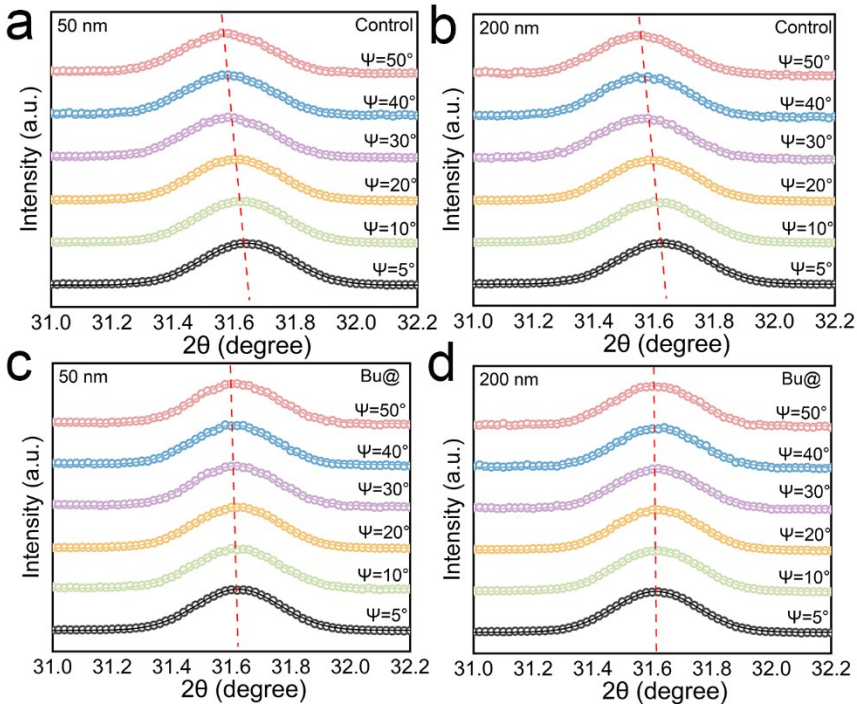

Figure S11. GIXRD spectra at different tilt angles (a-b) in the depth of 50 nm for a) control perovskite films. (b) Bu@-treated perovskite film. (c-d) in the depth of 200 nm for c) control perovskite films. (d) Bu@-treated perovskite film.

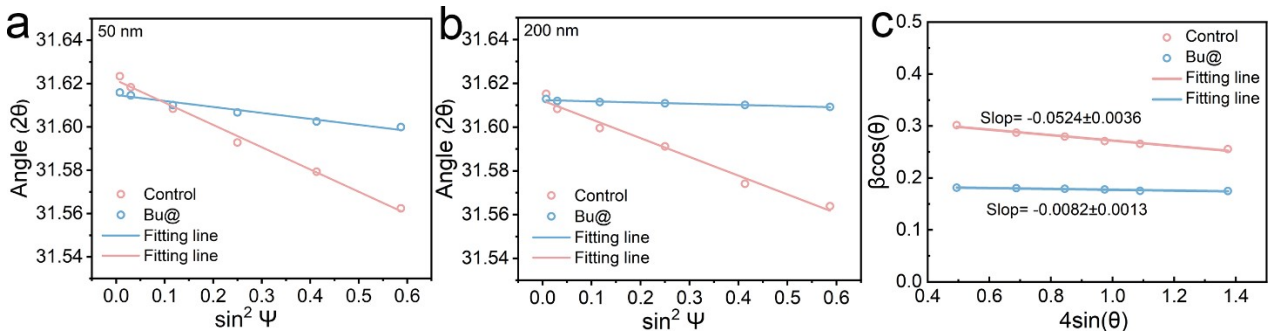

Figure S12. Linear fitting of the 2θ-sin^{2}Ψ of the GIXRD spectra at different depths of (a) 50nm and (b) 200nm. (c) Williamson-Hall plots obtained from XRD patterns of the perovskite films without and with Bu@ interlayer.

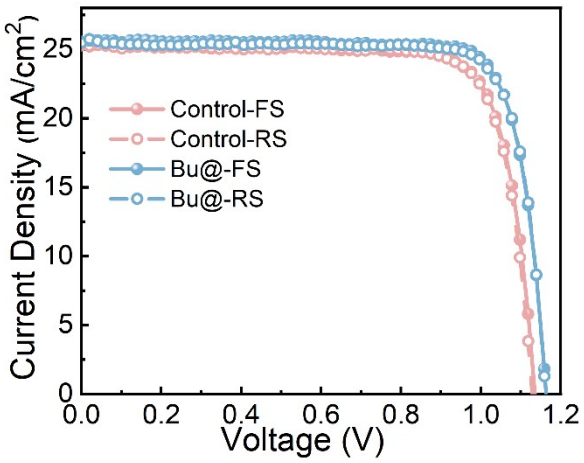

Figure S13. *J-V* curves of the champion devices with and without Bu@ interlayer measured in forward (solid line) and reverse (dashed line) voltage sweeping modes. The photovoltaic parameters are summarized in Table S6.

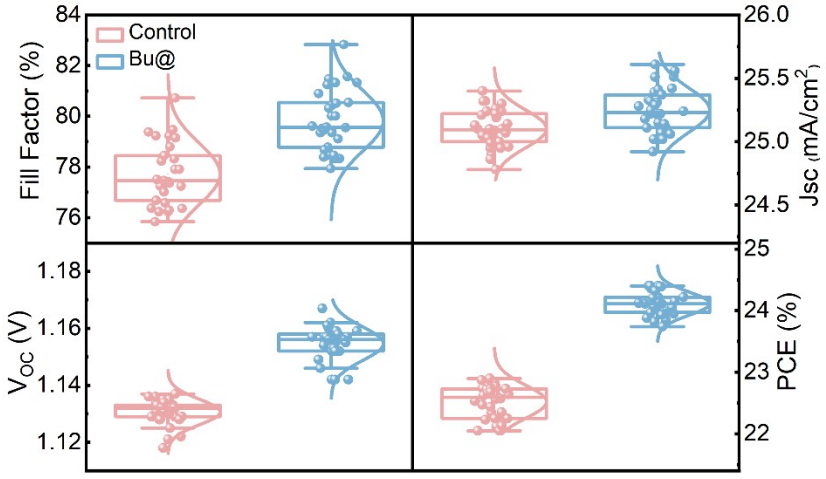

Figure S14. Statistics on the performance parameters (FF, J_{SC}, V_{OC}, PCE) of PSCs with and without Bu@ interlayer obtained from 30 devices for each system.

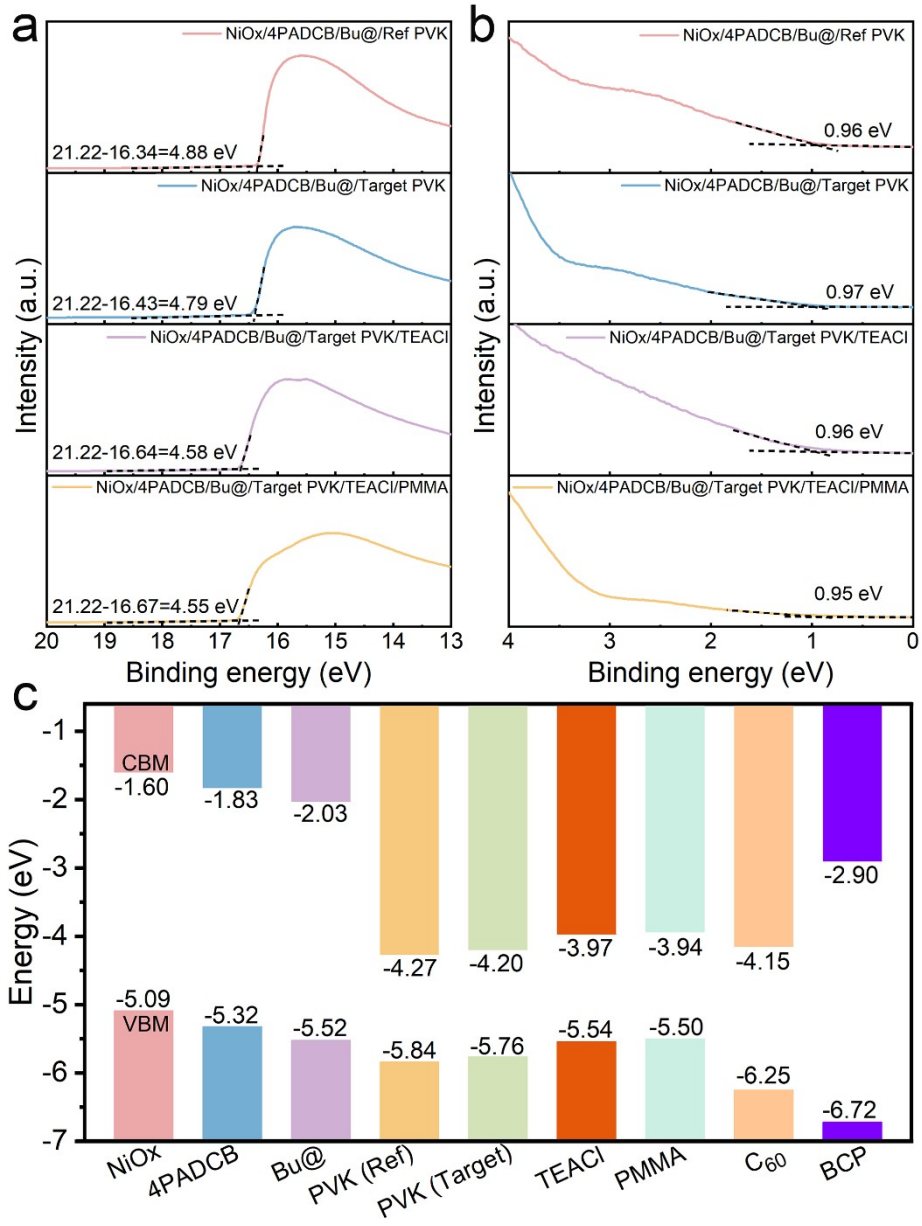

Figure S15. a. and b. UPS spectra of perovskite films and HTL layers with different modifications. c. Schematics of the energy alignment of individual layer.

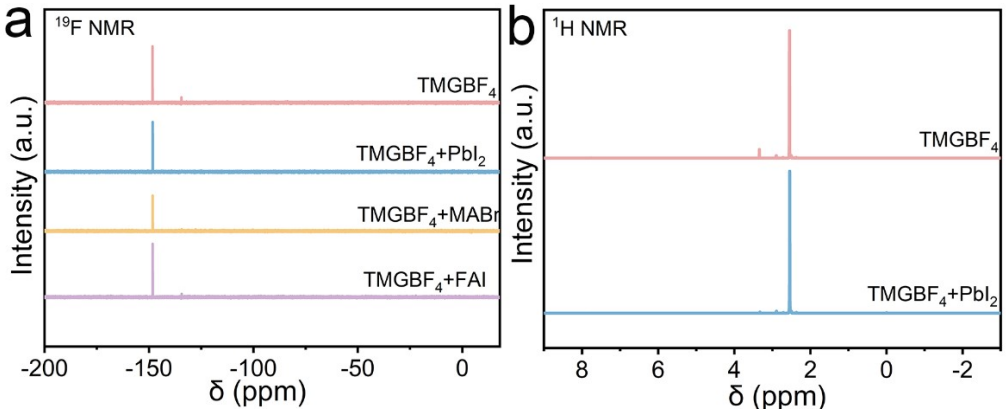

Figure S16. The proton nuclear magnetic resonance (a) ^{19}F NMR spectra. (b) ^{1}H NMR spectra of $TMGBF_4$ when mixed with PbI_2, FAI and MABr.

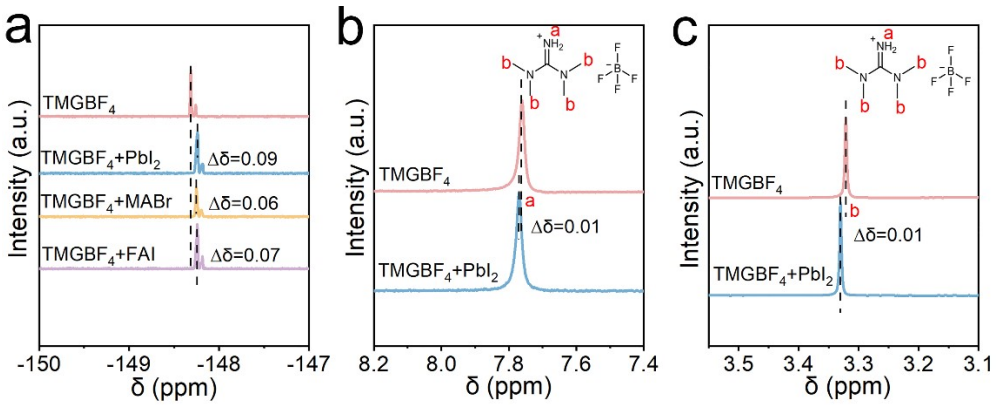

Figure S17. (a) ^{19}F NMR spectra of $TMGBF_4$ solution without or with additives. (b-c) ^{1}H NMR spectra of $TMGBF_4$ solution without or with PbI_2.

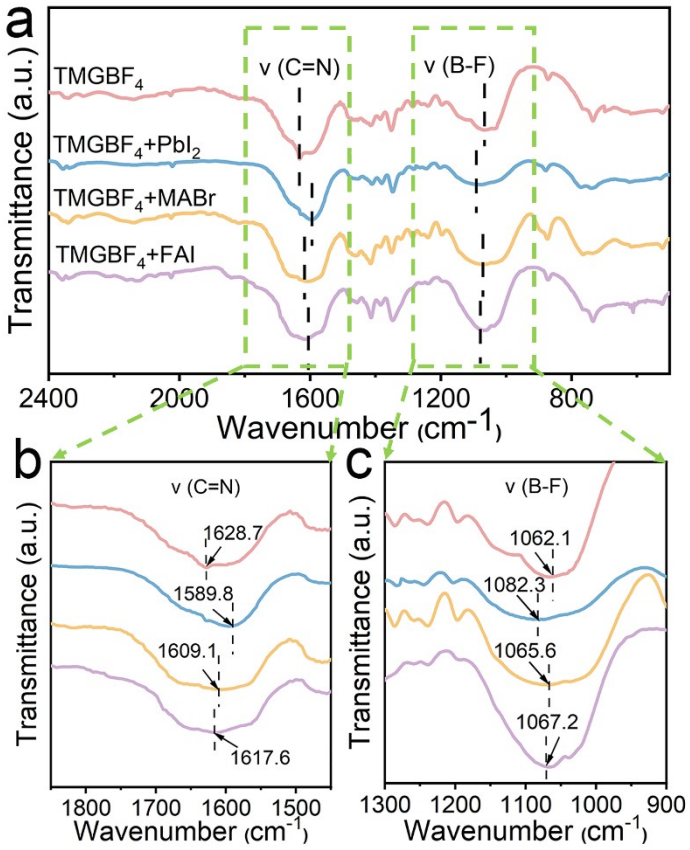

Figure S18. FTIR spectra of $TMGBF_4$ solution without or with additives.

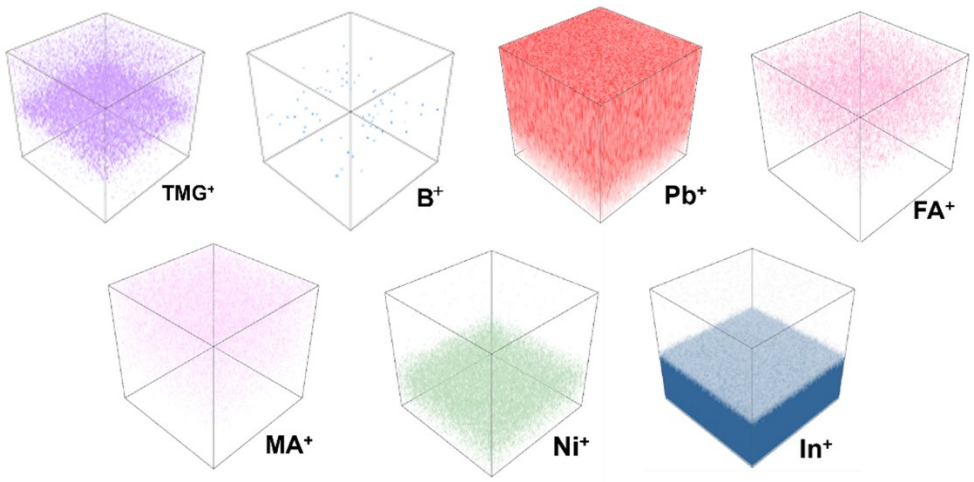

Figure S19. 3D images of unitary $TMGBF_4$-treated perovskite film. The tracked ions are all positively charged mono-valence fragments.

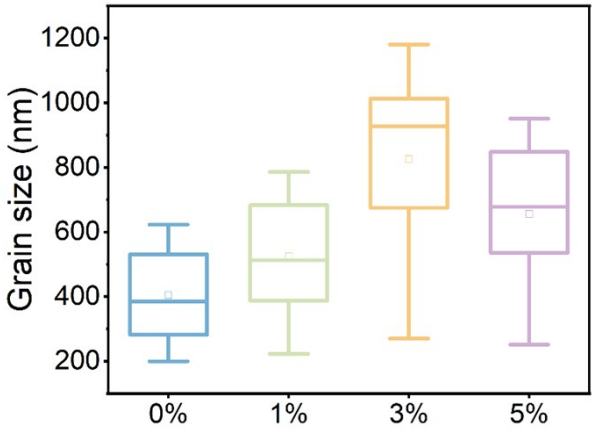

Figure S20. Grain size distribution in the perovskite films with different $TMGBF_4$ loadings (0, 1, 3 and 5%, mole percent with respect to PbI_2).

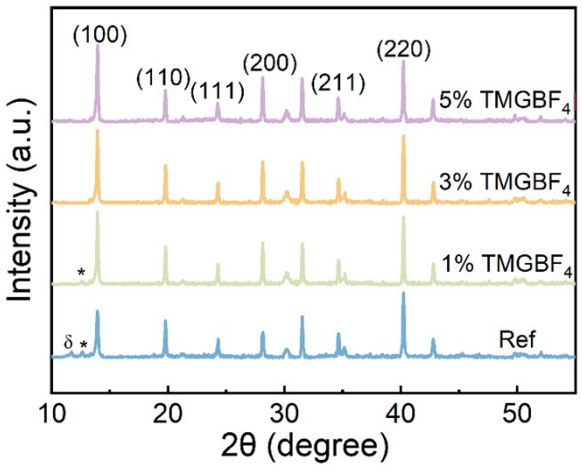

Figure S21. XRD patterns of the corresponding perovskite films.

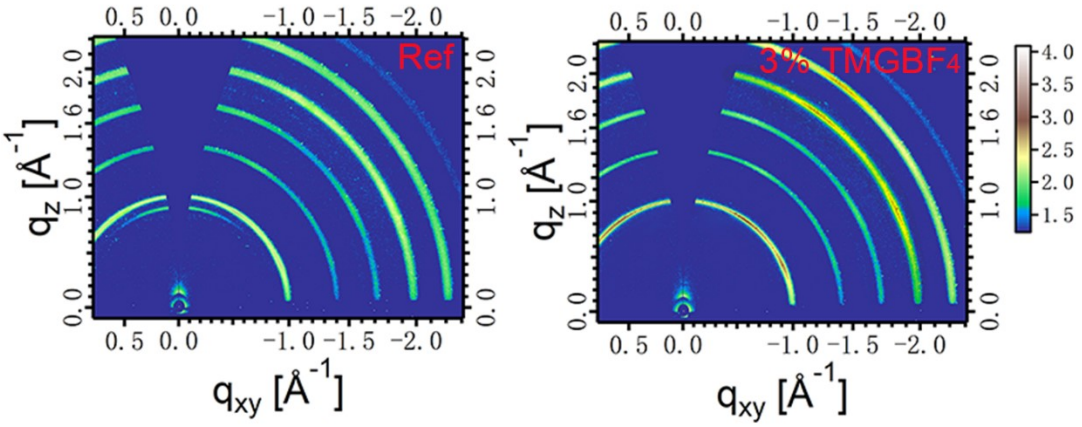

Figure S22. GIWAXS patterns reference and 3%$TMGBF_4$-treated perovskite films.

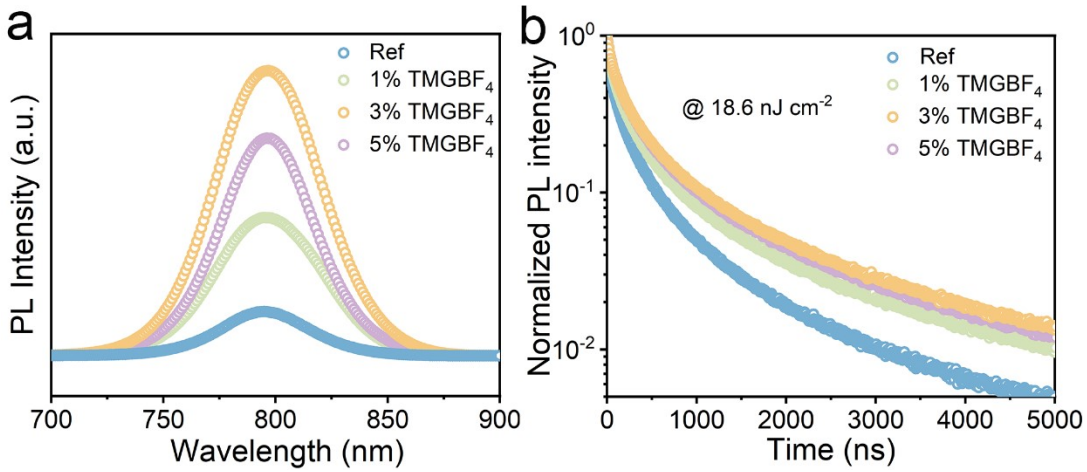

Figure S23. (a) Steady-state PL spectra. (b) TRPL spectra of the perovskite films with different $TMGBF_4$ additive content (0%, 1%, 3% and 5%) deposited on glass.

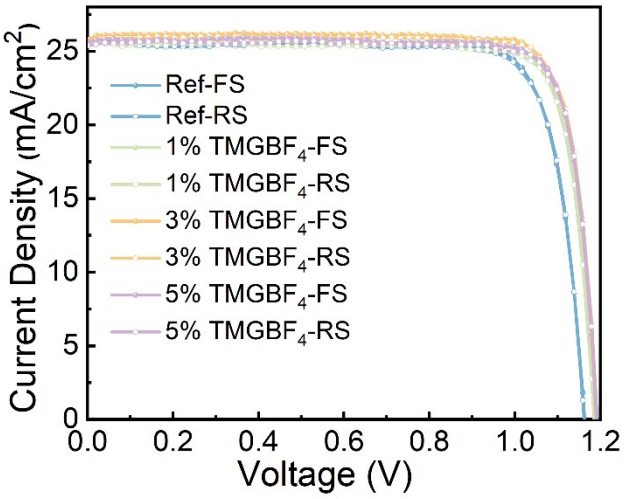

Figure S24. The *J-V* curves of the PSCs with different concentrations of $TMGBF_4$ additive. The photovoltaic parameters are summarized in Table S8.

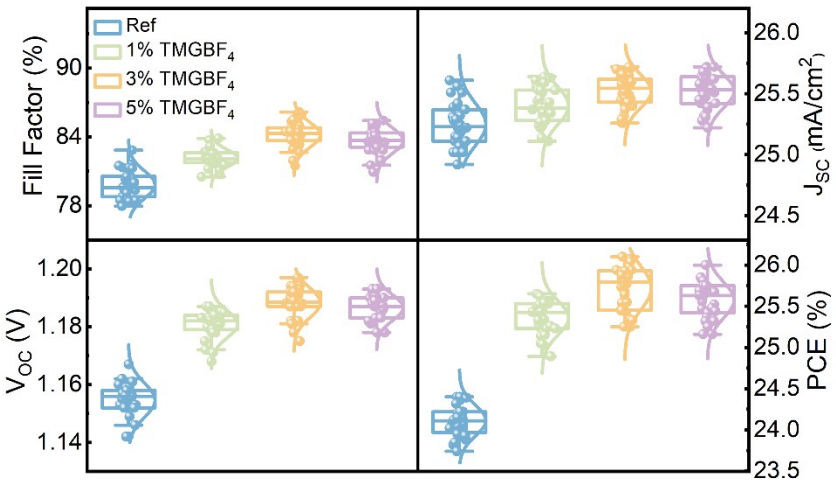

Figure S25. Statistics on the performance parameters of PSCs with different concentrations of $TMGBF_4$ (0%, 1%, 3% and 5%) obtained from 30 devices.

华南国家计量测试中心
广东省计量科学研究院
SOUTH CHINA NATIONAL CENTER OF METROLOGY
GUANGDONG INSTITUTE OF METROLOGY

校 准 证 书

CALIBRATION CERTIFICATE

证书编号 Certificate No. NYX202400312　　第 1 页，共 4 页 Page of

客户名称 Name of the Customer: Aung Ko Ko Kyaw Group, Southern University of Science and Technology

联络信息 Contact Information: 1088 Xueyuan Avenue, Nanshan District, Shenzhen, Guangdong, China

计量器具名称 Description: Inverted Perovskite Solar Cell

型号/规格 Model/Type: Inverted Perovskite Solar Cell

制造厂 Manufacturer: Aung Ko Ko Kyaw Group

出厂编号 Serial No.: 20240704 21-2 PSC　　设备管理编号 Equipment No.: ----

接收日期 Receipt on: 2024 年 Y 07 月 M 04 日 D

结论 Conclusion: 见校准结果 Shown in the results of calibration

校准日期 Calibration on: 2024 年 Y 07 月 M 04 日 D

发布日期 Issue on: 2024 年 Y 07 月 M 10 日 D

批 准 Authorized by: 周军红

核 验 Reviewed by: 周军红

校 准 Calibrated by: 梅书刚

华南国家计量测试中心 证书专用章

扫一扫查真伪

实验室地址：广东省东莞市石排镇东园大道石排段152号　邮政编码：523343
电话：(8620)86594172 传真：(8620)86590743 投诉电话：(8620)36611242 E-mail：scm@scm.com.cn
Add: No.1,Miaobianwang Section, Dongyuan Road South, Shipai Town, Dongguan, Guangdong.
Post Code: 523343 Tel: (8620)86594172 Fax: (8620)86590743 Complaint Tel: (8620)36611242
证书真伪查询：www.scm.com.cn；cert.scm.com.cn Certificate AuthenticityIdentify: www.scm.com.cn；cert.scm.com.cn

1

华南国家计量测试中心
广东省计量科学研究院
SOUTH CHINA NATIONAL CENTER OF METROLOGY
GUANGDONG INSTITUTE OF METROLOGY

校 准 结 果
RESULTS OF CALIBRATION

证书编号 NYX202400312 Certificate No.　　原始记录号 NYX202400312 Record No.　　第 3 页,共 4 页 Page of

一、外观检查： 符合要求

Apparent Inspectio Pass.

二、测试条件： 温度(25±2)℃；辐照度1000W/m^2。

Test conditions: Temperature: (25±2)℃; Irradiance: 1000W/m^2.

三、电流-电压曲线：

The IV curve:

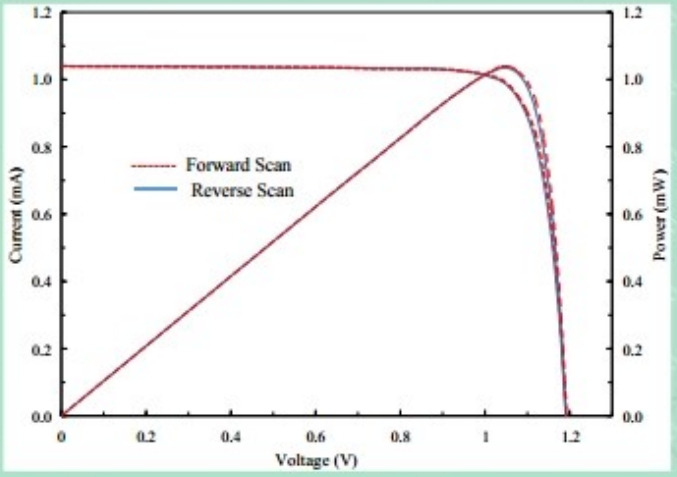

四、光电性能参数（正扫）：

Results of photoelectric properties (Forward Scan):

表1(Table 1)

短路电流密度J_{sc}	短路电流I_{sc}	开路电压V_{oc}	填充因子FF	最大功率P_m	最佳工作电流I_m	最佳工作电压V_m	转换效率η
Short ciruit current density	Short ciruit current	Open circuit voltage	Fill factor	Maximum power	Optimum working current	Optimum working voltage	Efficiency
mA/cm^2	mA	V	%	mW	mA	V	%
25.67	1.037	1.192	84.1	1.040	1.003	1.037	25.74

华南国家计量测试中心
广东省计量科学研究院
SOUTH CHINA NATIONAL CENTER OF METROLOGY
GUANGDONG INSTITUTE OF METROLOGY

校 准 结 果
RESULTS OF CALIBRATION

证书编号 NYX202400312 Certificate No.　　原始记录号 NYX202400312 Record No.　　第 4 页,共 4 页 Page of

五、光电性能参数（反扫）：
Results of photoelectric properties (Reverse Scan):

表2(Table 2)

短路电流密度J_{sc} Short ciruit current density	短路电流I_{sc} Short ciruit current	开路电压V_{oc} Open circuit voltage	填充因子FF Fill factor	最大功率P_m Maximum power	最佳工作电流I_m Optimum working current	最佳工作电压V_m Optimum working voltage	转换效率η Efficiency
mA/cm^2	mA	V	%	mW	mA	V	%
25.69	1.038	1.190	83.6	1.033	0.996	1.037	25.57

说明：
Note:
1、电池有效面积数据为0.0404 cm^2（有效面积基于金属掩模版面积）。
The effective area data of thecell is 0.0404 cm^2 (Effective area based on a metal aperture mask).
2、本次测量结果的扩展不确定度为：开路电压V_{oc}：U_{rel}=1.2%，短路电流I_{sc}：U_{rel}=2.7%，最大功率P_{max}：U_{rel}=3.0%，(k=2)。
The expanded uncertainty of measuring results: V_{oc}: U_{rel}=1.2%, I_{sc}: U_{rel}=2.7%, P_{max}: U_{rel}=3.0%, (k=2).
3、校准活动中对测量结果有影响的条件：温度:(25±2)℃ 湿度:(50±5)%RH。
Conditions under which the calibrations were made that have an influence on the measurement results:
Temperature:(25±2)℃ Humidity:(50±5)%RH.
4、本证书中给出的扩展不确定度依据JJF1059.1-2012《测量不确定度评定与表示》评定，由合成标准不确定度乘以包含概率约为95%时对应的包含因子k得到。
The expanded uncertainty given in this certificate is evaluated according to JJF 1059.1-2012"*Evaluation and Expression of Uncertainty in Measurement*",which is obtained by multiplying the combined standard uncertainty by the coverage factor k corresponding to the coverage probability of about 95%.
5、该仪器的溯源日期为本证书的“校准日期”，由于复校时间间隔的长短是由仪器的使用情况、使用者、仪器本身质量等诸因素所决定的，因此，送校单位可根据实际使用情况自主决定复校时间间隔。更换重要部件、维修或对仪器性能有怀疑时，应及时校准。
The traceability date of this instrument is the "Calibration Date"on this certificate, Since the calibration interval is determined by the use of the instrument,operation of the user, the quality of the instrument itself and other factors, the re-calibration date can decided by the user according to the actual situation. In case of replacement of important parts,maintenance or doubt on the performance of the instrument,it shall be calibrated in time.

Figure S26. Independent efficiency certification of perovskite solar cells by an accredited institute of South China National Center of Metrology, giving a PCE of 25.74% (short-circuit current (I_{SC}) of 1.037 mA, V_{OC} of 1.192 V and FF of 84.1%, forward scan) of the champion device.

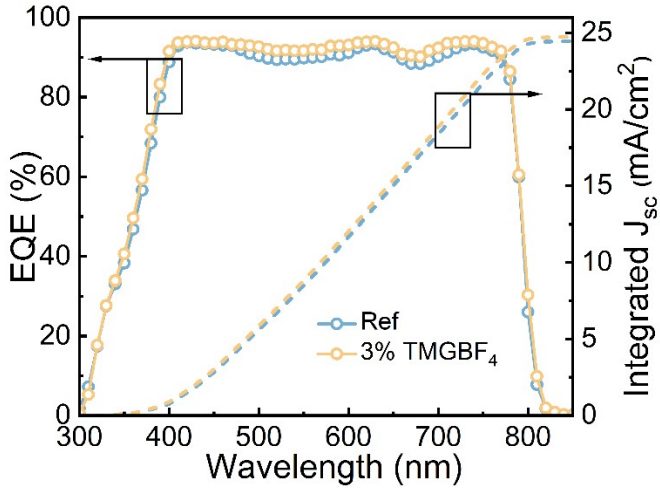

Figure S27. EQE spectra and the corresponding integrated J_{SC}.

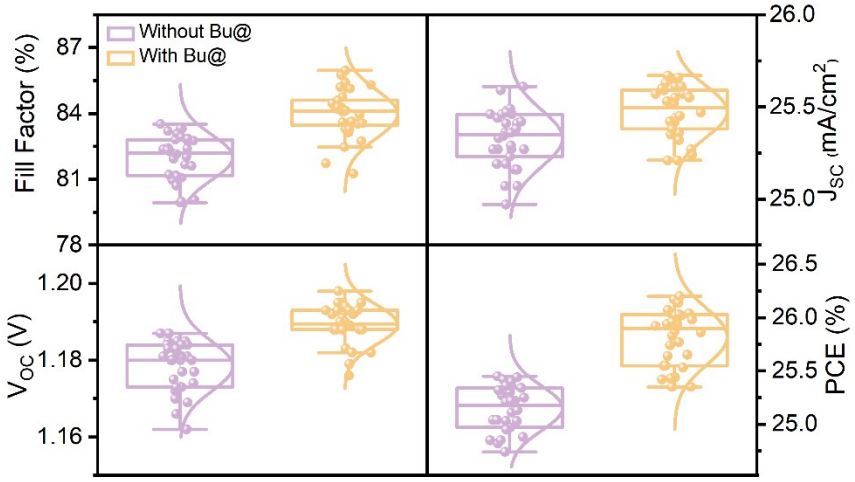

Figure S28. Statistics on the performance parameters of PSCs with and without Bu@ interface modification, while both are treated with $TMGBF_4$ obtained from 30 devices.

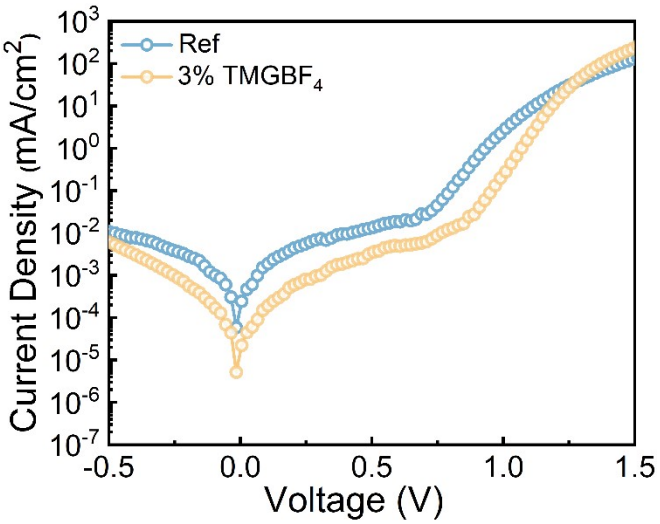

Figure S29. Dark *J-V* curves of the corresponding devices.

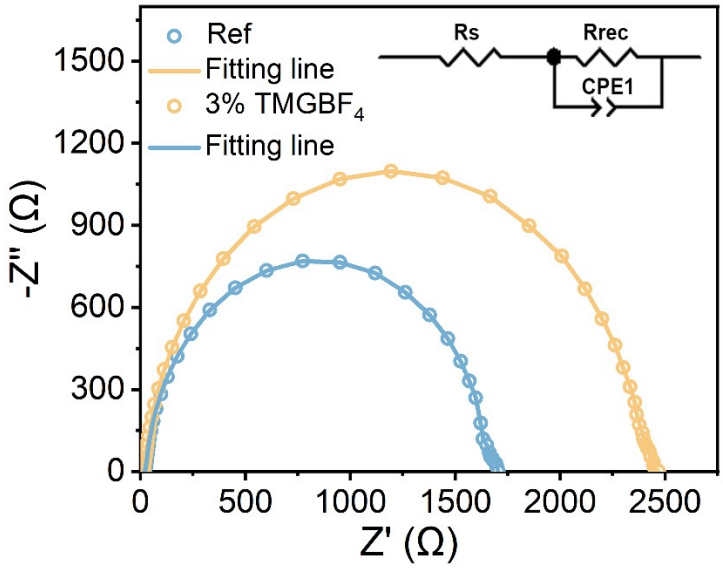

Figure S30. Nyquist plots of the corresponding devices. Inset shows its equivalent circuit.

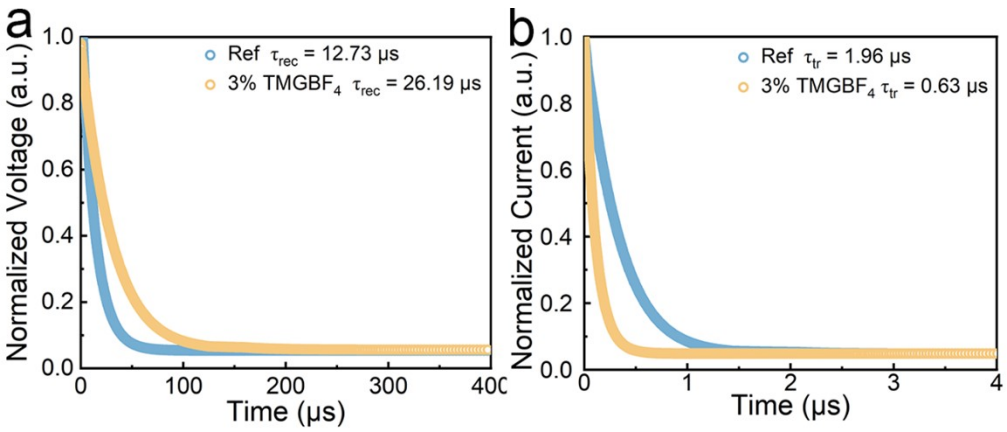

Figure S31. (a) TPV and (b) TPC spectra of the reference and the $TMGBF_4$-treated devices.

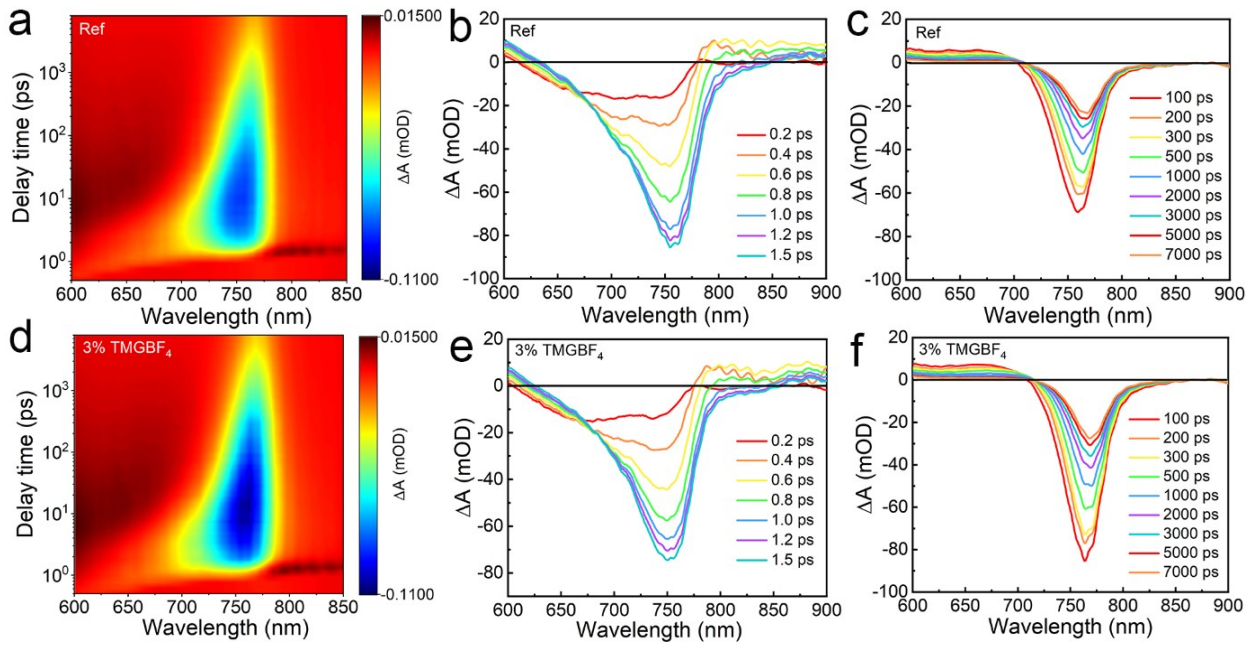

Figure S32. (a) and (d) The pseudo-color TA spectrum plot of reference and 3%$TMGBF_4$-treated perovskite films. (b) and (e) Delay time-dependent TA spectra (time scale: 0.2-1.5 ps) for reference and 3%$TMGBF_4$-treated perovskite films. (c) and (f) Delay time-dependent TA spectra (time scale: 100-7000 ps) for reference and 3%$TMGBF_4$-treated perovskite films.

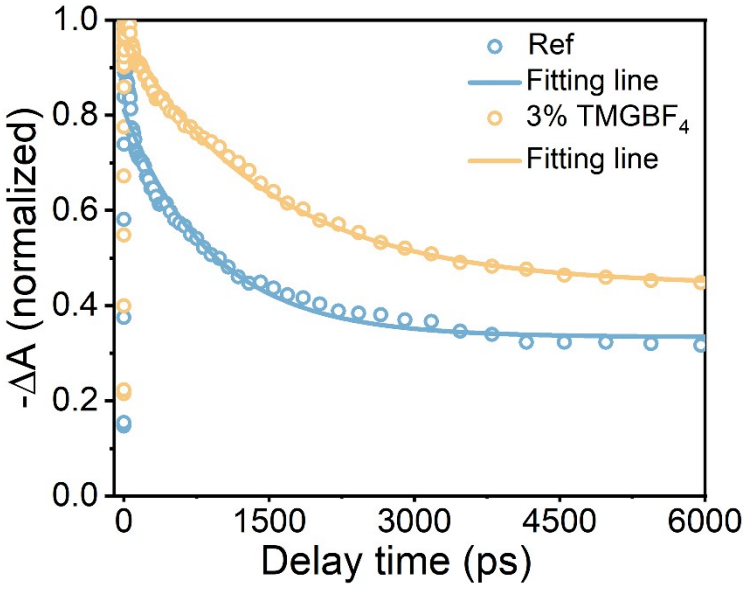

Figure S33. The bleach recovery kinetics for reference and the $TMGBF_4$-treated perovskite films

following the excitation at probe wavelength at 760 nm.

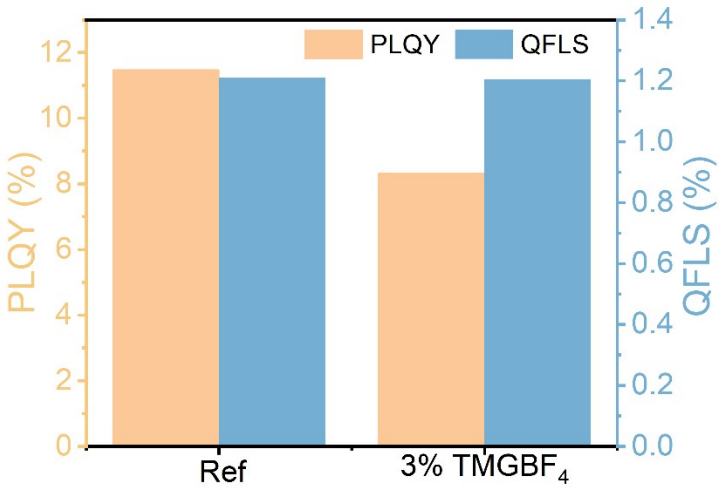

Figure S34. The PLQY measurements and calculated QFLS values of reference and $TMGBF_4$-treated samples.

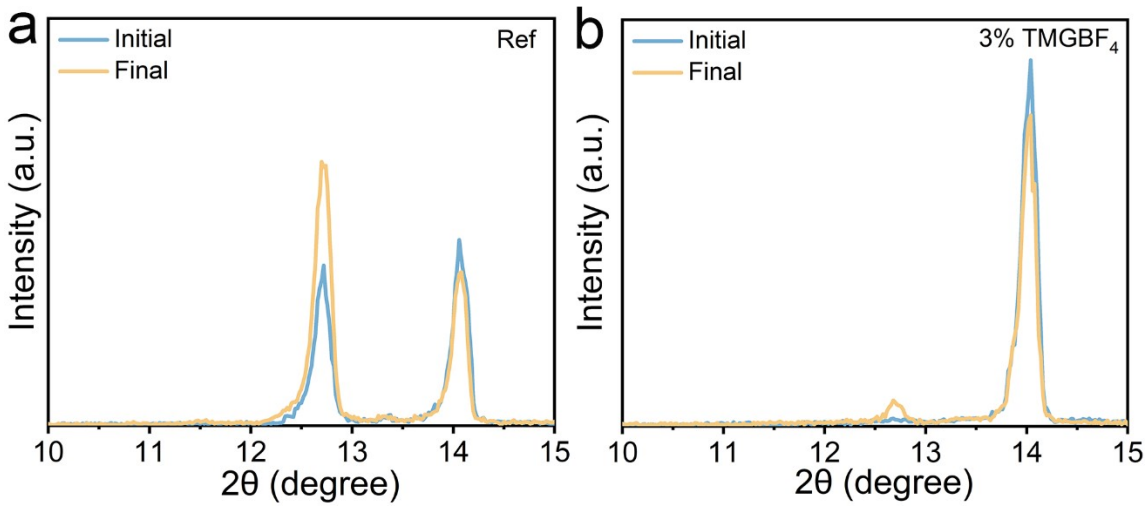

Figure S35. XRD patterns of (a) the reference and (b) $TMGBF_4$-treated perovskite films at the beginning (1minute) and ending (70 minutes) time under 150±5℃ in vacuum.

Table S1. The calculation data for relative content of hydroxide on different samples.

Samples		Hydroxide peak area	Lattice oxygen peak area	Deficiency area	Ratio (%)
ITO/4PADCB	Initial	2592.32	15515.93	10405.82	16.7
	DMF rinse	1102.23	14478.61	7779.13	7.6
	Methanol rinse	2035.66	12965.98	7615.73	15.7
ITO/4PADCB/Bu@	Initial	3477.42	22083.62	12462.69	15.6
	DMF rinse	2489.60	16062.38	7082.48	15.5

Table S2. Time-resolved PL data of perovskite films.

Samples	τ_1 (ns)	A_1(%)	τ_2 (ns)	A_2(%)	τ_{avg} (ns)
Glass/ITO/NiO_x/4PADCB//PVK	9.84	2.8	215.05	97.2	214.8
Glass/ITO/ NiO_x/4PADCB/ Bu@/PVK	82.46	1.7	676.83	98.3	675.5

The average lifetime (τ_{avg}) of perovskite films on quartz calculated with $\tau_{avg} = \frac{\sum_{i=1}^{n} A_i \tau_i^2}{\sum_{i=1}^{n} A_i \tau_i}$

Table S3. Instrumental angles (Ψ, ω, Φ) set for (012) crystal plane in different depths of GIXRD residual stress measurements.

Depth (nm)	(hkl)	Ψ (°)	ω (°)	Φ (°)
50	（012）	5	0.3114	-17.4592
		10	0.3151	-32.0793
		20	0.3303	-51.0211
		30	0.3588	-61.082
		40	0.4063	-66.8129
		50	0.4855	-70.3293
200	（012）	5	1.8318	-19.31
		10	1.8544	-34.9649
		20	1.95	54.2136
		30	2.1293	-64.0587
		40	2.4333	-69.7122
		50	2.9548	2.9548

Table S4. The slope of the residual strain fitting line and strain values for the perovskite films with and without $Bu(MIm)_2Br_2$ at the depth of 50 nm and 200 nm.

Depth (nm)	Films	Slope	Strain (MPa)
50	Control	-0.103±0.004	24.28±0.94
	Bu@	-0.054±0.003	12.73±0.70
200	Control	-0.086±0.002	20.26±0.47
	Bu@	-0.027±0.002	6.36±0.47

Table S5. Photovoltaic parameters for PSCs with or without $Bu(MIm)_2Br_2$ layer.

Device type	Scan direction	V_{OC} (V)	J_{SC} (mA/cm^2)	FF (%)	PCE (%)
Control	RS	1.135	25.44	78.92	22.80
	FS	1.129	25.29	79.64	22.72
Bu@	RS	1.164	25.55	81.93	24.36
	FS	1.162	25.47	81.75	24.20

Note: Forward scan and reverse scan were denoted as FS and RS, respectively.

Table S6. Time-resolved PL data of perovskite films with or without $TMGBF_4$.

Samples	τ_1 (μs)	A_1(%)	τ_2 (μs)	A_2(%)	τ_{avg} (μs)
Glass/ITO/0%$TMGBF_4$+PVK	0.193	0.90	0.844	99.1	0.842
Glass/ITO/1%$TMGBF_4$+PVK	0.464	1.4	1.048	98.6	1.044
Glass/ITO/3%$TMGBF_4$+PVK	0.493	2.4	1.221	97.6	1.268
Glass/ITO/5%$TMGBF_4$+PVK	0.291	1.8	1.273	98.2	1.216

Table S7. Photovoltaic parameters for PSCs with different concentrations of $TMGBF_4$.

Device type	Scan direction	V_{OC} (V)	J_{SC} (mA/cm^2)	FF (%)	PCE (%)
Ref	RS	1.164	25.55	81.93	24.36
	FS	1.162	25.47	81.75	24.20
1% $TMGBF_4$	RS	1.187	25.66	83.77	25.52
	FS	1.182	25.64	83.19	25.23
3% $TMGBF_4$	RS	1.192	25.78	85.21	26.18
	FS	1.193	25.67	84.70	25.94
5% $TMGBF_4$	RS	1.190	25.63	84.53	25.80
	FS	1.192	25.39	84.90	25.69

Note: Forward scan and reverse scan were denoted as FS and RS, respectively.

Table S8. The EIS fitting results of PSCs with different concentrations of $TMGBF_4$.

Device	R_s (Ω)	R_{rec} (Ω)	CPE_{T1} (F)	$CPEP_1$ (F)
Ref	5.19	3474	8.54×10^{-9}	0.9824
Target	1.80	4520	8.62×10^{-8}	0.9949

Supplementary References

1. H. Wang, C. Zhu, L. Liu, S. Ma, P. Liu, J. Wu, C. Shi, Q. Du, Y. Hao, S. Xiang, H. Chen, P. Chen, Y. Bai, H. Zhou, Y. Li and Q. Chen, *Adv Mater*, 2019, **31**, e1904408.
2. M. Ghasemi Hajiabadi, M. Zamanian and D. Souri, *Ceramics International*, 2019, **45**, 14084-14089.
3. C. Shan, T. Liu, J. Zhou, Y. He, D. Luo, Z. Jiang, Z. Wang, Q. Liu, C. a. Li, F. Zhang, E. Zhou, K. Wang and A. K. K. Kyaw, *Chemical Engineering Journal*, 2023, **471**.
4. R. Chen, J. Wang, Z. Liu, F. Ren, S. Liu, J. Zhou, H. Wang, X. Meng, Z. Zhang, X. Guan, W. Liang, P. A. Troshin, Y. Qi, L. Han and W. Chen, *Nature Energy*, 2023, **8**, 839-+.
5. S. Ye, H. Rao, Z. Zhao, L. Zhang, H. Bao, W. Sun, Y. Li, F. Gu, J. Wang, Z. Liu, Z. Bian and C. Huang, *Journal of the American Chemical Society*, 2017, **139**, 7504-7512.
6. Zhenyi Ni, Chunxiong Bao, Ye Liu, Qi Jiang, Wu-Qiang Wu, Shangshang Chen, Xuezeng Dai, Bo Chen, Barry Hartweg, Zhengshan Yu, Zachary Holman and J. Huang, *Science*, 2020, **6484**, 1352-+.
7. A. Ullah, K. H. Park, H. D. Nguyen, Y. Siddique, S. F. A. Shah, H. Tran, S. Park, S. I. Lee, K. K. Lee, C. H. Han, K. Kim, S. Ahn, I. Jeong, Y. S. Park and S. Hong, *Advanced Energy Materials*, 2021, **12**.